Published in final edited form as:
J Neurosci. 2013 January 23; 33(4): 1486–1497. doi:10.1523/JNEUROSCI.4269-12.2013.

Glutamatergic neurotransmission between the C1 neurons and the parasympathetic preganglionic neurons of the dorsal motor nucleus of the vagus

Seth D. DePuy[1,*], **Ruth L. Stornetta**[1], **Genrieta Bochorishvili**[1], **Karl Deisseroth**[2], **Ilana Witten**[3], **Melissa Coates**[1], and **Patrice G. Guyenet**[1]

[1]Department of Pharmacology, University of Virginia, Charlottesville, VA 22908

[2]Stanford University, Bioengineering & Psychiatry Depts. W083 Clark Center, 318 Campus Drive, Stanford, CA 94305

[3]1-S-16 Green Hall, Psychology Department, Princeton University, Princeton, NJ 08540

Summary

The C1 neurons are a nodal point for blood pressure control and other autonomic responses. Here we test whether these rostral ventrolateral medullary catecholaminergic (RVLM-CA) neurons use glutamate as a transmitter in the dorsal motor nucleus of the vagus (DMV). After injecting Cre-dependent AAV2 DIO-Ef1α-channelrhodopsin2(ChR2)-mCherry (AAV2) into the RVLM of dopamine-beta-hydroxylase Cre transgenic mice (DβH$^{Cre/0}$), mCherry was detected exclusively in RVLM-CA neurons. Within the DMV >95% mCherry-immunoreactive (-ir) axonal varicosities were tyrosine hydroxylase-ir and the same proportion were vesicular glutamate transporter 2 (VGLUT2)-ir. VGLUT2-mCherry co-localization was virtually absent when AAV2 was injected into the RVLM of DβH$^{Cre/0}$;VGLUT2$^{flox/flox}$ mice, into the caudal VLM (A1 noradrenergic neuron-rich region) of DβH$^{Cre/0}$ mice or into the raphe of ePet$^{Cre/0}$ mice. Following injection of AAV2 into RVLM of TH-Cre rats, phenylethanolamine N-methyl transferase (PNMT) and VGLUT2 immunoreactivities were highly co-localized in DMV within EYFP-positive or EYFP-negative axonal varicosities. Ultrastructurally, mCherry terminals from RVLM-CA neurons in DβH$^{Cre/0}$ mice made predominantly asymmetric synapses with ChAT-ir DMV neurons. Photostimulation of ChR2-positive axons in DβH$^{Cre/0}$ mouse brain slices produced EPSCs in 71% of tested DMV preganglionic neurons (PGNs) but no IPSCs. Photostimulation (20 Hz) activated PGNs up to 8 spikes/sec (current clamp). EPSCs were eliminated by tetrodotoxin, reinstated by 4-aminopyridine and blocked by ionotropic glutamate receptor blockers. In conclusion, VGLUT2 is expressed by RVLM-CA (C1) neurons in rats and mice regardless of the presence of AAV2, the C1 neurons activate DMV parasympathetic preganglionic neurons monosynaptically and this connection uses glutamate as an ionotropic transmitter.

Introduction

The C1 neurons are a subset of catecholaminergic neurons that reside at the rostral end of the ventrolateral medulla and, in rats, express the adrenaline-synthesizing enzyme phenylethanolamine N-methyl transferase (PNMT) (Hokfelt et al., 1974; Ross et al., 1983). Their contribution to the regulation of sympathetic vasomotor tone and blood pressure is

Address correspondence to: Patrice G. Guyenet, PhD, University of Virginia Health System, P.O. Box 800735, 1300 Jefferson Park Avenue, Charlottesville, VA 22908-0735. Tel: (434) 924-7433; Fax: (434) 982-3878; pgg@virginia.edu.
*current address: University of Chicago, Institute for Integrative Physiology, Center for Systems Biology, 5841 South Maryland Avenue MC5068, Room N- 701, Chicago, Illinois 60637-1470.

thoroughly documented and is attributed to their direct projections to the intermediolateral cell column (Ross et al., 1983; Guyenet, 2006; Abbott et al., 2009b; Marina et al., 2011). Less known is the fact that the C1 neurons also have dense axonal projections to the dorsal motor nucleus of the vagus, DMV (Hokfelt et al., 1974; Card et al., 2006). This connection suggests that the C1 neurons may also regulate the parasympathetic component of the autonomic nervous system. A major objective of this study is to test this hypothesis and to identify whether the input from the C1 cells to the DMV is monosynaptic and excitatory.

Contrary to most brainstem noradrenergic neurons, adult C1 neurons in rats contain readily detectable levels of vesicular glutamate transporter 2 (VGLUT2) mRNA (Stornetta et al., 2002) and the cognate protein is present within PNMT-ir terminals presumed to originate from these neurons (Rosin et al., 2006; Card et al., 2006). Conversely, >90% of C1 neurons lack a plasmalemmal monoamine transporter (Lorang et al., 1994; Comer et al., 1998) and there is yet no direct evidence that their axonal terminals release catecholamines (Sved, 1989). PNMT-ir varicosities, unlike those of dopaminergic neurons, typically make conventional synapses in adult rats (Milner et al., 1988; 1989; Moss et al., 2011; Berube-Carriere et al., 2012). These predominantly asymmetric synapses are structurally reminiscent of forebrain glutamatergic synapses. However, evidence that adult C1 cells release glutamate is based on in vivo pharmacology, therefore of an indirect nature (Morrison et al., 1989; Abbott et al., 2009a; 2012). In sum, the C1 cells appear to be excitatory and could be using glutamate as one of their transmitters but definitive evidence is lacking.

In the present study we used a combination of neuroanatomical and electrophysiological approaches to test whether adult RVLM-CA neurons form conventional excitatory glutamatergic synapses with DMV neurons in mice. Channelrhodopsin-2 (ChR2) was selectively introduced into the RVLM-CA neurons by injecting a Cre-dependent adeno-associated virus into the rostral ventrolateral medulla of transgenic mice that express Cre recombinase exclusively in dopamine-beta-hydroxylase (DβH)-containing neurons (Stornetta et al., 2012). We examined whether the axonal varicosities of the RVLM-CA neurons contain VGLUT2 and whether these terminals form conventional synapses with vagal preganglionic neurons. We used TH-Cre transgenic rats (Witten et al., 2011) to verify some of the mouse findings and to ascertain that the axonal projections from the C1 cells to the DMV possess VGLUT2-ir varicosities regardless of whether the C1 neurons had been exposed to AAV2. Finally, we recorded from vagal parasympathetic preganglionic neurons in slices of adult mice and examined the effects produced by photostimulating the ChR2-expressing nerve fibers originating from the RVLM-CA cells.

Materials and Methods

Animals

Animal use was in accordance with guidelines approved by the University of Virginia Animal Care and Use Committee. All electrophysiology experiments were done using 21 $D\beta H^{Cre/0}$ mice (9 females, 12 males). Histology experiments were done with 13 $D\beta H^{Cre/0}$ mice (7 males, 6 females). DβH-Cre mice were obtained from the Mutant Mouse Regional Resource Center at the University of California, Davis, CA, USA [Tg(Dbh-cre)KH212Gsat/Mmcd; stock # 032081-UCD]. The transgenic line was maintained as hemizygous (Cre/0) on a C57BL/6J background. $Vglut2^{(flox/flox)}$ mice (JAX Stock #012898; STOCK $Slc17a6^{tm1Lowl/J}$)(Tong et al., 2007) maintained as homozygous (flox/flox) were bred with DβH-Cre mice to generate $D\beta H^{Cre/0}$; $VGlut2^{flox/0}$ and subsequently crossed with $Vglut2^{flox/flox}$ for 2 generations to generate DβH-$Cre^{(Cre/0)}$; $Vglut2^{(flox/flox)}$ mice in which VGLUT2 should be absent from any Cre-expressing noradrenergic or adrenergic neurons. Three of these $D\beta H^{Cre/0}$; $Vglut2^{flox/flox}$ mice (2 females, 1 male) were also used for histology experiments. Histology experiments were also conducted on 3 $ePet^{Cre/0}$ mice (2

males, 1 female) kindly provided by E.S. Deneris, (Case Western Reserve University) (Scott et al., 2005) and 5 TH $^{Cre/0}$ rats (all males, rat line obtained from Ilana Witten (Princeton University) and Karl Deisseroth, (Stanford University) (Witten et al., 2011) and maintained as hemizygous (Cre/0) on a Long-Evans background. All animals were at least 8 weeks old at time of AAV2 injection.

AAV2 vectors

DIO-eF1α-ChR2-mCherry AAV serotype 2 and DIO-eF1α-EYFP AAV serotype 2 (Atasoy et al., 2008) were obtained from the University of North Carolina Vector core (Chapel Hill, NC) (AAV2 titer: 10^{12} viral molecules per ml).

Stereotaxic injections of AAV2 into the rostral ventrolateral medulla of mice or rats

DβH-Cre and DβH$^{Cre/0}$; Vglut2$^{flox/flox}$ and ePet$^{Cre/0}$ mice were anesthetized with a mixture of ketamine (100 mg/kg) and dexmedetomidine (0.2 mg/kg) given i.p. and received three injections of undiluted DIO-eF1α-ChR2-mCherry AAV2 (360 nl total volume) into the left RVLM, the left caudal VLM (A1 catecholaminergic region) or the raphe obscurus after methods previously described (Depuy et al., 2011; Stornetta et al., 2012).

TH-Cre rats were anesthetized with a mixture of ketamine (75 mg/kg), xylazine (5 mg/kg) and acepromazine (1 mg/kg). A total of 500 nl of DIO-eF1α-EYFP AAV2 was injected in three RVLM locations aligned in the longitudinal direction using methods previously described (Abbott et al., 2012).

In vitro electrophysiology

Four to twelve weeks after AAV2 injection, DβH$^{Cre/0}$ mice were anesthetized with a mixture of ketamine (120mg/kg) and xylazine (12mg/kg) given i.p., then decapitated. The brainstem was removed and sectioned into 300 μm slices in the transverse plane in ice-cold, N-Methyl-D-glucamine (NMDG)-substituted artificial cerebral spinal fluid (ACSF) containing (in mM): 92 NMDG, 2.5 KCl, 1.25 NaH_2PO_4, 10 $MgSO_4$, 0.5 $CaCl_2$, 20 HEPES, 30 $NaHCO_3$, 25 glucose, 2 thiourea, 5 Na-ascorbate, 3 Na-pyruvate (~300 mOsm/kg). After 10 minutes at 33°C, brain slices were transferred to aerated physiological extracellular ACSF containing (in mM): 119 NaCl, 2.5 KCl, 1.25 NaH_2PO_4, 2 $MgSO_4$, 2 $CaCl_2$, 26 $NaHCO_3$, 12.5 glucose, 2 thiourea, 5 Na-ascorbate, 3 Na-pyruvate and maintained at room temperature (23–25 °C). All recordings were performed at room temperature in submerged slices continuously perfused with aerated physiological ACSF.

The transverse slices from which DMV neurons were recorded included the area postrema or were immediately adjacent to this level in either direction. To record postsynaptic currents (PSC), electrodes (2–6 MΩ tip resistance) were filled with an intracellular solution containing (in mM): 140 Cs-methanesulfonate, 10 HEPES, 10 tris-phosphocreatine, 3 ATP-Na, 0.3 GTP-Na, 1 EGTA, 2 $MgCl_2$ (pH 7.3). The calculated E[Cl-] was −88mV. EPSCs were recorded at Vhold of −70mV (−79.4 mV after junction potential correction). IPSCs were recorded at Vhold of 0 mV (−9.4 mV after junction potential correction).

For current clamp recordings a similar pipette solution was used replacing Cs-methanesulfonate with K-gluconate (junction potential 14.8 mV). Corrected membrane potentials are reported in the text and figures. Biocytin-filled electrodes were used to label the recorded cells intracellularly in 7 experiments. Whole-cell voltage-clamp and current-clamp recordings were performed on visually identified DMV neurons (68 neurons in total). Three mice received an injection of Fluoro-Gold (FG) (5 ml/kg of 1% solution in sterile water (Fluorochrome LLC, Denver, CO), i.p.) and 8 FG neurons were recorded in these

mice. These neurons responded exactly as the DMV neurons selected on the basis of location only and the results were pooled.

Recordings were performed using a Multiclamp 700B amplifier and pClamp 10 software (Molecular Devices, Inc., Sunnyvale, CA, USA). Signals were low-pass filtered at 4 kHz and digitized at 10 kHz. Only cells with series resistance that remained below 25MΩ were included in the analysis.

For photostimulation of ChR2 terminals, the tip of a 200 μm diameter optical fiber coupled to a 473nm DPSS laser (IkeCool Corporation, Anaheim, CA) was placed ~300μm away from the DMV. Delivery of optical pulses (1 ms duration) was controlled by a digitizer (Digidata 1440A, Molecular Devices) controlled by episodic protocols run in pClamp 10 (Molecular Devices). The laser/fiber was calibrated for 5 mW steady-state output prior to each experiment.

Histology

Perfusions—All animals receiving AAV2 injections and used exclusively for histology (both mice and rats) survived 4–6 weeks after injections and were anesthetized (pentobarbital overdose) and perfused transcardially first with heparinized saline and then with 4% paraformaldehyde (pf) (mice with 10 ml saline, then 80 ml pf and rats with 100 ml saline and then 400 ml pf) and brains removed and postfixed in 4% pf for 2 to 5 days. For ultrastructural analysis, 5 of the AAV2-injected DβH-Cre mice were anesthetized as above and perfused transcardially with 20 ml of heparinized saline (1,000 U/ml) followed by fixative ((25 ml of 2% paraformaldehyde with 3.75% acrolein (Electron Microscope Sciences), followed by 30 ml of 2% paraformaldehyde). Brains from these animals were removed and post-fixed for at least 3 hours in 2% paraformaldehyde before sectioning.

Recorded brain slices—After recording, the slices that contained biocytin-filled neurons were transferred to 4% paraformaldehyde for 2–5 days at 4°C.

FG injections—Four 4–6 week old C57Bl6/J mice received i.p. injections of 200 μl of 1% FG. After 3–5 days, the mice were deeply anesthetized and perfused. Brains were removed, postfixed in 4% paraformaldehyde for up to 5 days. Brains were sectioned and reacted for immunohistochemistry as described below.

Sectioning and immunohistochemistry—Thirty micron-thick transverse sections were cut through the DMV with a vibrating microtome (Leica) and collected into a cryoprotectant solution and stored at −20 °C before further processing. All histological procedures were done with free-floating sections. Sections were rinsed, blocked and incubated in primary antibodies (TH, ChAT, FG, dsRed, PNMT, VGLUT2 as previously described (Bochorishvili et al., 2011; Stornetta et al., 2012)). Sections were then rinsed and incubated for 45–60 min in appropriate secondary antibody, then rinsed, mounted on gelatinized glass slides, dehydrated through a graded series of alcohols and covered with DPX. Slides were examined using a Zeiss Axioskop2 and photographed with a Zeiss MRC camera (Bochorishvili et al., 2011; Stornetta et al., 2012). Ultrastructural procedures were done exactly as described by Bochorishvili et al. (2011).

Statistical analysis

All data were analyzed using the GraphPad Prism v5.04 statistical package. Statistical significance ($P<0.05$) was determined using parametric ANOVA (one-way or repeated measures) with post hoc Student-Newman-Keuls, or non-parametric analysis with Kruskal-Wallis (Dunn's post hoc) or Wilcoxon signed rank test. Before statistical analysis, normality

of distribution was determined with the Kolmogorov-Smirnov test and homogeneity of variance was tested with Bartlett's test. Unless stated otherwise, data are expressed as mean ± SEM.

Results

ChR2-mCherry labeled terminals originating from RVLM-catecholaminergic (RVLM-CA) neurons innervate the dorsal motor nucleus of the vagus (DMV) and contain VGLUT2

The location of the neurons that expressed ChR2-mCherry following injection of DIO-ChR2-mCherry AAV2 was examined in five mice that were also used for ultrastructural analysis of labeled terminals within the DMV. Consistent with our previous study in which we utilized the same electrophysiologically guided procedure to inject the vector into the rostral portion of the ventrolateral medulla (RVLM) (Stornetta et al., 2012), the mCherry-immunoreactive (ir) neurons were confined to the RVLM, mostly caudal to the facial motor nucleus (Fig. 1A). The mCherry-positive neurons were 97% ± 1% tyrosine hydroxylase (TH)-ir, hence potentially catecholaminergic (Fig. 1B).

In all mice, the DMV contained a dense network of mCherry-ir terminals that made close appositions with choline acetyl-transferase (ChAT)-ir, i.e. cholinergic neurons (Fig. 1C,D).

Evidence that neurons recorded in the DMV were parasympathetic preganglionic cells

We confirmed that these DMV cholinergic neurons were parasympathetic preganglionic neurons by showing that all these cholinergic neurons contained FG in mice that had received an intraperitoneal (ip) injection of this retrogradely transported dye. After i.p. injection of FG in 3 animals, neurons labeled with FG within the DMV were counted and the proportion of FG-labeled DMV neurons that were immunoreactuve for choline-acetyl transferase (three sections per mouse) was determined. The coincidence was 95.1 ± 1.5%, (total of 1219 neurons counted, example in Fig. 2A1–A3). Brainstem slices were made from an additional 3 mice injected i.p. with FG and 8 FG-positive DMV neurons cells were recorded and filled with biocytin as described (example in Fig. 2B1–B3). The extensive filling with biocytin allowed for computer-assisted reconstruction of the dendrites and axonal processes of four cells (2 examples shown in Fig. 2C) showing a long, presumably axonal, process exiting along the expected trajectory for a parasympathetic preganglionic neuron.

Since almost all mCherry-expressing cells in the RVLM of DIO-ChR2-mCherry AAV2 injected animals were TH-ir, we expected that a similarly high proportion of the mCherry-ir terminals located in the DMV would also be TH-ir but the ChR2-containing axons present in the DMV could conceivably have originated primarily from the very few TH-negative hence apparently non-catecholaminergic neurons that expressed the transgene. To exclude this possibility, in three $D\beta H^{Cre/0}$ mice injected with AAV2, coronal sections were reacted for simultaneous immunofluorescent detection of TH and mCherry and we counted singly (mCherry-ir) and dually-labeled axonal varicosities (both mCherry and TH-ir) in the region of the DMV outlined in Fig. 3A, which also corresponds to the region that was explored electrophysiologically. In this region, most (98.6 ± 0.2%) of the mCherry-positive axonal varicosities were TH-ir (Fig. 3 B1–B3; 1370 total terminals counted in 3 sections, one section per mouse). Parallel experiments were done to determine what proportion of the ChR2-expressing axonal varicosities contained VGLUT2 immunoreactivity in the same region of the DMV. Most (97 ± 1 %) mCherry-ir axonal varicosities were also VGLUT2-ir (Fig. 3 D1–D3; 1950 total terminals counted in 3 sections, one section per mouse). On statistical grounds, this evidence demonstrates that most ChR2 axonal varicosities contain both VGLUT2 and TH immunoreactivities. By performing triple-label experiments, we

were able to find direct evidence of the presence of all three markers (mCherry, VGLUT2 and TH) within the same terminals in the DMV although the degree of coincidence was not quantified (Fig. 3 C1–C3).

Control experiments were done to verify that we correctly identified the presence of VGLUT2 in the terminals of the RVLM-CA neurons and to exclude the possibility that the presence of VGLUT2 might be an artifact caused by AAV2 transduction. In 3 DβH$^{Cre/0}$ mice, DIO-ChR2-mCherry AAV2 was injected more caudally within the ventrolateral medulla where the A1 group of noradrenergic neurons resides. In rats, very few A1 neurons contain VGLUT2 mRNA suggesting that they are not glutamatergic (Stornetta et al., 2002). The cell bodies of these caudal VLM catecholaminergic neurons expressed high levels of transgene (not shown). These cells also projected to the dorsal vagal complex and adjacent nucleus of the solitary tract but very few of their axonal varicosities (8.7 ± 1.5 %) were also VGLUT2-ir (Fig. 3E1–E3; 567 total terminals counted in one section each from 3 mice). In the second control group, we injected the same amount of DIO-ChR2-mCherry AAV2 into the raphe obscurus of three ePet $^{Cre/0}$ mice, a procedure that results in selective expression of the transgene by serotonergic neurons (Scott et al., 2005; Depuy et al., 2011). These serotonergic neurons also abundantly innervated the dorsal vagal complex. Most of their varicosities were not VGLUT2-ir (Fig. 3F1–F3). Only 7.4 ± 1% of the mCherry-ir terminals originating from these raphe neurons appeared VGLUT-ir (1137 terminals counted from one section each of 3 mice). The third control group consisted of 3 DβH-Cre$^{Cre/0}$; VGLUT2$^{flox/flox}$ mice that received the standard injections of DIO-ChR2-mCherry AAV2 in the C1 region. The DMV of these mice contained approximately the same density of mCherry-ir axonal projections as the control (DβH$^{Cre/0}$) mice but only 8.2 ± 3.2% of the mCherry varicosities were also VGLUT2-ir (Fig. 3 G1–G3). In summary, within the mouse dorsal motor nucleus of the vagus, the axonal varicosities of the RVLM-CA neurons (presumptive C1 cells) typically contained both TH and VGLUT2, whereas very few terminals from A1 noradrenergic and raphe obscurus serotonergic neurons exposed to the same AAV2 contained VGLUT2. The absence of VGLUT2 in serotonergic neurons conforms to expectation since this particular vesicular transporter is not known to be expressed by these neurons in adult tissue (Gras et al., 2002). The small number of VGLUT2-positive terminals originating from A1 and raphe could conceivably be false positive results caused by the close juxtaposition of two terminals from different neurons and likely represents the “background”. Finally, we demonstrated the selectivity of the immunohistochemical detection of VGLUT2 within the varicosities emanating from RVLM-CA cells by showing that VGLUT2 immunoreactivity was present only at “background” level when the Cre-dependent vector was injected into DβH$^{Cre/0}$; VGLUT2$^{flox/flox}$ mice.

The final light microscopy histological experiments were conducted in TH-Cre rats and had three goals. One was to test whether the projection from RVLM-CA neurons to DMV also exists in rats and is also glutamatergic. The second goal was to verify that this projection emanates from the C1 (PNMT-positive) neurons. To do so we located the adrenaline-synthesizing enzyme PNMT that is diagnostic of the C1 neurons and is co-expressed with TH and DβH in these neurons (Phillips et al., 2001). The third goal was to verify, in rats, that AAV2 does not reactivate a latent glutamatergic phenotype in these catecholaminergic neurons, a possibility raised previously to explain discrepancies between electrophysiological results suggesting a contribution of glutamate to neurotransmission in adult mesolimbic dopaminergic neurons and the lack of supportive ultrastructural evidence (Stuber et al., 2010; Moss et al., 2011; Berube-Carriere et al., 2012). We injected DIO eF1α EYFP AAV2 into the RVLM of 3 TH-Cre rats, which caused a high level of expression in PNMT-ir neurons (typical injection site shown in Fig. 4A). EYFP was also detected in a smaller number of RVLM neurons devoid of PNMT immunoreactivity suggesting some degree of ectopic Cre recombinase expression (data not illustrated). Numerous triple-labeled

terminals containing EYFP, VGLUT2 and PNMT immunoreactivities were observed in each rat within the DMV (Fig. 4B). Within this structure almost all PNMT-ir terminals were also VGLUT2-ir whether or not they were labeled with EYFP suggesting that AAV2 transduction could not have explained the presence of VGLUT2 in PNMT-ir terminals. To further verify this point, we examined the DMV of two TH-Cre rats that had not been injected with AAV2. Virtually all PNMT-ir terminals identified within the DMV were also VGLUT2-ir (Fig. 4C). In summary, RVLM-CA neurons also innervate the DMV in rats. As in mice, the axonal projections of these neurons to the DMV contain VGLUT2 and the presence of VGLUT2 in these neurons is not an artifact caused by AAV2 transduction.

ChR2-mCherry labeled terminals from RVLM-CA neurons make monosynaptic contacts with cholinergic DMV neurons

We identified 113 mCherry-ir (DAB-labeled) profiles within the DMV using tissue from 5 mice processed for EM. The DMV region examined is specified in Fig. 3A. These profiles consisted exclusively of unmyelinated axons and nerve terminals. Immunogold-silver labeling for ChAT was observed only within perikarya and dendrites. In tissue dually labeled for mCherry and ChAT we identified 65 synaptic contacts between mCherry-ir varicosities and ChAT-ir profiles (Fig. 5 A–D, Table 1). The majority of these synapses (N =48, 74%) were asymmetric (Fig. 5A–D) but 17 symmetric axodendritic or axosomatic synapses also were detected (26%; Fig. 5E). A small proportion of mCherry-positive boutons made synaptic contact onto dendrites that lacked detectable immunoreactivity for ChAT (n=18; 12 asymmetric and 6 symmetric contacts). Because ChAT immunodetection was restricted to the surface of the sections, these negative results are not clearly interpretable. They could either be false-negative results or denote that, within the confines of the DMV, RVLM-CA neurons also innervate neurons other than the parasympathetic preganglionic neurons.

Dense core vesicles consistent with catecholamine-releasing organelles were detected within the more lightly labeled mCherry-positive varicosities (Fig. 5F) but most terminals contained a level of peroxidase reaction product that was too high to reliably observe such vesicles.

Photostimulation of RVLM-CA terminals in the DMV evokes postsynaptic inward currents in DMV neurons

DMV neurons were recorded in brain slices prepared from adult $D\beta H^{Cre/0}$ mice approximately one month after injection of AAV2-DIO-ChR2-mCherry into RVLM. The dorsal vagal complex from AAV2-injected mice contained mCherry-positive fibers that were clearly visible (observed with epifluorescence using Zeiss filter set 20: excitation 546 nm, emission 575 nm). The slices used for recording did not contain mCherry-positive somata, confirming that few if any A1 noradrenergic neurons had been exposed to the AAV2. mCherry-positive somata were consistently observed in the expected ventrolateral medullary location in more rostral slices.

We believe that we recorded exclusively from DMV neurons because of their fairly obvious location in coronal slices. Moreover, in several instances when we recorded from DMV neurons visualized with Fluoro-Gold, we obtained the same results as with DMV neurons sampled without Fluoro-Gold guidance. Also, several intracellular fills labeled DMV neurons with an axon that extended mediolaterally towards an exiting vagal rootlet (Fig. 2) as expected for parasympathetic preganglionic neurons. Finally, the membrane potential and discharge characteristics of the DMV neurons recorded in current clamp were similar to those reported previously (Browning et al., 1999; Martinez-Pena y Valenzuela et al., 2004).

Blue light (473 nm, 5mW, 1ms pulses) was delivered by placing a 200 μm thick optical fiber 300 μm above the dorsal vagal complex. The light pulses had no detectable effect in DMV neurons prepared from naïve mice (7 DMV neurons clamped at −79.4mV). In contrast, the light produced EPSCs (or EPSPs) in 71% of the DMV neurons recorded from AAV2-injected DβH-Cre mice (48 of 68 cells; 21 mice). The electrophysiological effects produced by the light were therefore ChR2-dependent. Low frequency light pulses (1ms, 0.5Hz) evoked a compound, inward postsynaptic current (PSC) in most DMV neurons clamped at a holding potential of −79.4 mV (Fig. 6A1, A2). PSCs were elicited with a latency of 5.5 ± 0.3ms (23 neurons) from laser onset and had an amplitude of 71.3 ± 17.6pA (13 neurons). When the PSC was of small amplitude (<60 pA), occasional failures were observed (Fig. 6A1). When the evoked PSC had a larger amplitude (60–120 pA; Fig. 6B1,B2), it was more prominently multiphasic and a PSC after-discharge lasting nearly a full second (decay τ = 0.6s) was commonly observed (Fig. 6B3).

High frequency photostimulation (1ms, 20Hz, 5s), produced a very large increase in PSC frequency with a concurrent inward shift in the holding current (Fig. 6C1). Unlike with the single pulse paradigm, the PSCs elicited by train stimulation occurred at random relative to the laser pulses (Fig. 6C1: *stim*). Accordingly, during train stimulation, stimulus-triggered waveform averages were flat (Fig. 6C2). Train stimulation almost always produced a strong after-discharge of PSCs that took greater than 30 seconds to return to the pre-stimulus (baseline) frequency (Fig. 6C1: *afterdischarge*; Fig. 6D). PSCs were binned in 10s intervals following the end of the photostimulus and between groups differences were determined by non-parametric Friedman's analysis (F=87.4; P<0.0001) followed by Dunn's post hoc test for multiple comparisons (see Fig. 6D). The decay in PSC frequency following a train of stimuli could be modeled with two exponentials (τ_{fast}=2.3 ± 0.4 s; τ_{slow}=48 ± 18 s, N=16 neurons).

We also recorded from DMV neurons in whole-cell current-clamp mode to determine whether the excitatory input from RVLM-CA neurons was strong enough to elicit action potentials. On average, DMV neurons had a resting membrane potential of −63 ± 1.5mV (N = 7) and a baseline-firing rate of 0.8 ± 0.2Hz. In every recorded cell (N = 8), photostimulation of RVLM-CA terminals using a 5-second train (1ms, 20Hz) of laser light bursts produced a massive increase in EPSP frequency and markedly increased the resting discharge rate of the recorded neuron. The DMV neuron illustrated in Figure 6E1,E2 was kept just below firing threshold by injection of bias current (−10 pA) and the first differential of the original voltage recording (dV/dt) is shown as a means of better distinguishing the occurrence of postsynaptic potentials. In the 7 cells in which no bias current was applied, discharge rate was increased from 0.8 ± 0.3 spikes/s to 3.7 ± 0.8 spikes/s (p<0.01, paired t-test).

Photostimulation of ChR2-expressing RVLM-CA terminals elicits excitatory PSCs exclusively

Photostimulation (5s trains, 1 ms, 5 mW) was performed while the DMV neurons were clamped at two discrete holding potentials to differentiate excitatory, cationic currents (inward; Vm = −79.4 mV) from inhibitory, anionic currents (outward; Vm = −9.4mV; representative examples in Fig. 7A1, B1). At Vm of −79.4 mV the photostimulus train produced a barrage of inward, short-lasting EPSCs (decay τ = 6.5 ± 0.3ms; amplitude = 12.7 ± 1.8pA; N = 8; Fig. 7A1,A2,C). When the neuron was clamped at Vm= −9.4 mV, longer-lasting outward IPSCs (decay τ = 16.5 ± 1.1ms; amplitude = 20.7 ± 1.5pA; n=8) were typically observed during the resting period, but the frequency of these events was unaffected by photostimulation (Fig. 7B1,B2,C). At rest the recorded DMV neurons received an approximately equal frequency of EPSCs and IPSCs (Fig. 7C). Two-way repeated-measures ANOVA followed by Bonferroni post hoc test for multiple comparisons

indicated that only EPSC frequency was altered during photostimulation. Influence of photostimulation; $F(2,32)=54.43$, $P<0.0001$. Influence of PSC (EPSC vs. IPSC); $F(1,16)=8.56$, $P<0.01$. Interaction of photostimulation and PSC; $F(2,32)=51.2$, $P<0.0001$.

Thus, based on this sample of 8 neurons, photostimulation of the axons of RVLM-CA neurons does not elicit IPSCs in DMV neurons. The absence of detectable mRNA transcripts for glycine transporter 2 or glutamic acid decarboxylase in RVLM-CA neurons in rats agrees with these findings (Stornetta and Guyenet, 1999; Stornetta et al., 2004).

The EPSCs evoked in DMV neurons by stimulating RVLM-CA terminals are glutamatergic

The strong increase in EPSC frequency and associated inward shift in membrane current elicited by trains of photostimuli (1 ms, 20 Hz, 5s) in DMV neurons clamped at −79.4mV was unchanged by the addition of bicuculline and strychnine to block GABA and glycine–mediated currents, leaving the total integrated current (area under the curve, AUC) during the stimulus period unchanged (Fig. 8A2). However, addition of the NMDA/AMPA antagonists AP5/CNQX produced near complete blockade of spontaneous EPSCs and EPSCs elicited during the photostimulation (Fig. 8A1–A2). Group data were analyzed with one-way ANOVA for repeated measures, $(F(2,6)=7.7$; $P<0.05)$ followed by Student-Newman-Keuls (SNK) post hoc test for multiple comparisons. The AP5/CNQX mixture also greatly attenuated the peak amplitude (93.1 ± 2.6%) and integrated AUC (91.1 ± 2.4%) of the averaged compound EPSC evoked by single pulse photostimulation (1ms, 0.5Hz; N = 4; not illustrated). The broad spectrum excitatory amino acid antagonist kynurenic acid (1 mM) reversibly reduced background EPSC activity and also markedly attenuated the inward current generated by the trains of photostimuli (1 ms 20 Hz, 5s; 82.3 ± 3.9% attenuation; $P<0.01$; Fig. 8B1–B2). Like AP5/CNQX, kynurenic acid also significantly reduced the peak amplitude and integrated AUC of the EPSCs elicited by low frequency stimulation (respectively 66.2 ± 4.4% and 72.7 ± 4.1% attenuation; $P<0.01$; N = 9; not illustrated). Group data for effects of kynurenic acid were analyzed by one-way ANOVA for repeated measures, $(F(2,22)=7.8$; $P<0.01)$ followed by SNK post hoc test for multiple comparisons.

Glutamatergic input from RVLM-CA neurons to DMV neurons is monosynaptic

To determine if the excitatory glutamatergic input from RVLM-CA neurons to the DMV was mono- or poly-synaptic, we first blocked voltage-gated sodium (Na_v) channels with 1μM tetrodotoxin (TTX), then we applied 100 μM 4-aminopyridine (4-AP) to block the K_v channels that are critical for the repolarization of the axon (Shu et al., 2007). This protocol eliminates action potential-dependent, therefore potentially polysynaptic events, but enhances the direct depolarization of ChR2-positive terminals and the local release of neurotransmitter during photostimulation (Petreanu et al., 2009). As found by the latter authors, the compound EPSC evoked by single-pulse stimulation (1ms, 0.5Hz) was virtually eliminated by TTX (Fig. 9A,B). After co-application of TTX and 4-AP, a slower, ChR2-dependent EPSC that relied on glutamate transmission was reinstated (Fig. 9A,B). Group data were analyzed by the non-parametric Kruskal-Wallis test $(H=14.3$, $P<0.01)$ followed by Dunn's post hoc test for multiple comparisons. Use of a 5-second train of stimuli (1 ms, 20 Hz) produced similar results (Fig. 9C). Application of TTX alone significantly blunted the overall response to train stimulation. The increase in evoked EPSCs was delayed and only at the very end of the 5-second stimulus period did a small increase in EPSC frequency become apparent. This suggested that TTX imposed a significant slowing of the terminal depolarization during the photostimulus, requiring seconds to reach a "threshold" for Ca^{2+} entry and vesicular docking. Co-application of TTX and 4-AP restored the response towards the control value, particularly the rapid increase in EPSCs occurring early in the stimulus train (Fig. 9C). This action potential-independent transmission relied on ionotropic glutamate receptors as blockade with NMDA/AMPA antagonists eliminated the effect of

photostimulation (Fig. 9C,D). Group data were analyzed by one-way ANOVA, $F(3.21)=17.8$, $P<0.0001$) followed by SNK post hoc test for multiple comparisons. The number of repeats per group is unequal due to loss of recorded neurons at different points along the experiments. Significance of comparisons: CNQX/AP5 vs. control and TTX vs. control, $p<0.001$. 4AP vs. control, $p<0.01$. CNQX/AP5 vs. TTX/4AP and TTX vs. 4AP, $p<0.05$. CNQX/AP5 vs. TTX, n.s.

Discussion

This study provides the first direct evidence that the C1 cells make excitatory glutamatergic synapses in the adult brain. We also show that these neurons, better known for their contribution to sympathetic tone generation, activate parasympathetic premotor neurons in the dorsal vagal complex.

Monosynaptic glutamatergic input from the C1 cells to the DMV: anatomical evidence

We show here that, within the DMV, the axonal varicosities of the catecholaminergic neurons located in the RVLM contain VGLUT2 immunoreactivity in both rats and mice. Importantly, we show that VGLUT2 immunoreactivity correctly identified the presence of VGLUT2 protein because it was no longer detectable in DβH-$Cre^{Cre/0}$; $Vglut2^{flox/flox}$ mice. Few axonal varicosities originating from the presumed A1 noradrenergic cells or from raphe obscurus serotonergic neurons were detectably VGLUT2-ir consistent with the lack of VGLUT2 mRNA in serotonin neurons and relative paucity of VGLUT2 mRNA in A1 neurons (Stornetta et al., 2002). In short, as in the rat, RVLM-CA neurons have a glutamatergic phenotype. Although we were not able to identify PNMT in the RVLM-CA neurons of mice, the CNS projections of these neurons are virtually identical to those of the C1 cells in rats (Card et al., 2006; Stornetta et al., 2012).

The present ultrastructural study shows that RVLM-CA neurons establish conventional synapses with DMV neurons. The predominantly asymmetric morphology of these synapses is consistent with prior ultrastructural studies of PNMT-ir terminals in rats (Milner et al., 1988; 1989). In the forebrain, asymmetric synapses are associated with ionotropic glutamatergic transmission (Sheng and Kim, 2011). The significance of the 25% symmetric synapses between RVLM-CA neurons and DMV neurons is elusive. The postsynaptic thickening could have been missed for lack of serial sectioning. The existence of a subset of RVLM-CA neurons that do not use glutamate as a transmitter is possible.

Monosynaptic input from the C1 cells to the DMV neurons: electrophysiological evidence

Photostimulation of slices from control mice had no effect on DMV neurons and photostimulation had no effect in 30% of DMV neurons in the experimental mice. The electrophysiological effects produced by photostimulation therefore required expression of ChR2.

Although the recorded DMV neurons received on average an approximately equal frequency of spontaneous inhibitory and excitatory PSCs, photostimulation of ChR2-expressing fibers evoked EPSCs exclusively. These EPSCs were unaffected by adding glycinergic and $GABA_A$ receptor blockers but were greatly attenuated by administration of blockers of ionotropic glutamate receptors such as kynurenate or a mixture of CNQX and AP5. This evidence indicates that the PSCs evoked by photostimulating the C1 axons were mediated primarily by glutamate.

Consistent with the ultrastructural results, the glutamatergic input from the C1 cells to the DMV is monosynaptic since EPSCs could still be evoked by photostimulating the ChR2-labelled terminal field when fast sodium channels were blocked by tetrodotoxin (TTX) and

these EPSCs reappeared after addition of 4-aminopyridine, a potassium blocker that prolongs the depolarization of the terminals and reinstates vesicular release (Petreanu et al., 2009). Finally the reinstated PSCs were blocked by the combination of CNQX and AP-5 demonstrating their glutamatergic nature.

In summary, photostimulation of the axonal processes of RVLM-CA neurons elicited EPSCs in a substantial proportion of DMV preganglionic neurons. These EPSCs were monosynaptic and glutamatergic. Fast evoked IPSCs were not found, consistent with the absence of GAD or GlyT2 mRNA in RVLM-CA neurons (Stornetta and Guyenet, 1999; Stornetta et al., 2004).

Is the release of glutamate by the C1 neurons an injury response caused by the adeno-associated virus?

Cultured dopaminergic neurons make glutamatergic synapses (Sulzer et al., 1998) and, based on evidence similar to ours, others (Tecuapetla et al., 2010; Stuber et al., 2010) have proposed that the dopaminergic neurons that innervate nucleus accumbens also use glutamate as an excitatory transmitter in adult mice. Consistent with this evidence, VGLUT2 mRNA is present in TH-ir neurons within the A10 region (Yamaguchi et al., 2011). Yet, careful ultrastructural studies have failed to detect the presence of VGLUT2 in the dopaminergic varicosities of adult mice (Moss et al., 2011). These negative anatomical findings could mean that glutamate and dopamine are stored and released by separate varicosities (Broussard, 2012). A more disturbing possibility would be that adeno-associated vectors somehow injure adult dopaminergic neurons and reinstate a glutamatergic phenotype that these cells only express early during development or in culture (Berube-Carriere et al., 2009). A similar explanation seems highly unlikely in the case of the C1 neurons for the following reasons. First, the AAV2 did not induce VGLUT2 in noradrenergic (A1) or serotonergic neurons. We did find a very low percentage of mCherry terminals that appeared to contain VGLUT2 in these control experiments in mice but this percentage was the same regardless of whether the transgene was expressed by noradrenergic (A1) or serotonergic cells, therefore a technical artifact is the more likely explanation. Second, in the absence of AAV2, most rat C1 cells contain VGLUT2 mRNA (Stornetta et al., 2002). Third, we did observe VGLUT2 and TH-ir doubly-labeled terminals that were not transduced with mCherry in the DMV of the DBH-Cre RVLM-injected mice. Fourth, we showed that, in TH-Cre rats, the terminals of the C1 neurons, identified within the DMV by PNMT immunohistochemistry were VGLUT2-ir regardless of whether or not they arose from C1 neurons that were AAV2-transfected. Fifth, unlike the mesencephalic dopaminergic neurons (Berube-Carriere et al., 2012), the C1 neurons commonly make conventional synapses with thickened postsynaptic densities reminiscent of glutamatergic excitatory synapses, in rats (Milner et al., 1988; 1989) and in mice (present study). Finally, the notion that the C1 neurons use glutamate as one of their transmitters is consistent with numerous pharmacological observations *in vivo* (Morrison et al., 1989; Abbott et al., 2012). In sum, we found no evidence suggesting that AAV2 induces the synthesis of VGLUT2 in the C1 cells nor in medullary noradrenaline or serotonergic neurons. Our conclusion is that the C1 neurons of adult rodents normally express this transporter and use glutamate as an ionotropic transmitter, at least in the DMV.

Do the C1 neurons release catecholamines?

The C1 neurons presumably also release catecholamines inclusive of adrenaline since they express all the enzymes necessary for the synthesis and vesicular storage of these bioamines (Armstrong et al., 1982; Sevigny et al., 2008) but supportive neurophysiological evidence is lacking and the present experiments were not designed to explore this aspect of C1 neuron biology. We did observe dense core vesicles in the more lightly labeled synaptic boutons

originating from the C1 cells but dense core vesicles also store peptides which are plentiful in C1 cells (Chalmers et al., 1987; Halliday et al., 1988; Stornetta et al., 1999; Farnham et al., 2008). The C1 neurons express on their soma α_2-adrenergic receptors that are negatively coupled to calcium and potassium conductances (Li et al., 1995; Li et al., 1998). These autoreceptors may mediate autoinhibition or autocrine regulations analogous to those found in non-neural cells such as the endothelium and macrophages (Engler et al., 2005; Sorriento et al., 2012). The catecholamines released by the C1 cells could also activate presynaptic autoreceptors like the CNS noradrenergic neurons (Trendelenburg et al., 2003). Adrenaline is a β2-adrenoceptor-selective agent that facilitates transmitter overflow in sympathetic neurons and could conceivably exert a similar effect in C1 cells (Stjarne and Brundin, 1976).

In sum, our study demonstrates the existence of a strong glutamatergic component to synaptic transmission between the C1 cells and DMV neurons. The circumstances under which C1 neurons release catecholamines and the contribution of these substances to C1 neuron signaling remain to be determined.

Physiological implications of the innervation of DMV neurons by the C1 cells

The contribution of the C1 cells to blood pressure and sympathetic tone regulation is well established. It is partly the result of the massive projections of these neurons to the intermediolateral cell column and lamina X and likely involves glutamate signaling (Ross et al., 1983; 1984; Guyenet, 2006). C1 neurons also regulate adrenaline release by the adrenal glands (Ritter et al., 1998; 2001; Li et al., 2009) and subsets of C1 neurons innervate the paraventricular nucleus of the hypothalamus and regulate the CRF-ACTH-corticosterone cascade (Sawchenko et al., 2000).

The present study indicates that the DMV is another synaptic target of the C1 neurons. DMV neurons regulate liver metabolism, gastrointestinal function including motility and secretions, immune responses and probably cardiac function (Standish et al., 1995; Rogers et al., 1999; Olofsson et al., 2012). A broad spectrum of these parasympathetic efferents is likely to be targeted by a subset of C1 cells given that two thirds of randomly sampled DMV neurons responded to photostimulation of their axons.

Given that C1 cells are activated by various stressors (Pirnik et al., 2004) and have been implicated in the cardiovascular response to stress (Chen et al., 2012), the C1 neurons, via their synaptic inputs to the DMV, may also be at least partially responsible for the negative digestive and immunological consequences of stress.

Acknowledgments

This work was supported by the following grants from the National Institutes of Health (HL28785 and HL74011 to PGG, 1F32HL096280-01 to SDD).

REFERENCES

Abbott SB, Kanbar R, Bochorishvili G, Coates MB, Stornetta RL, Guyenet PG. C1 neurons excite locus coeruleus and A5 noradrenergic neurons along with sympathetic outflow in rats. J Physiol. 2012; 590:2897–2915. [PubMed: 22526887]

Abbott SB, Stornetta RL, Socolovsky CS, West GH, Guyenet PG. Photostimulation of channelrhodopsin-2 expressing ventrolateral medullary neurons increases sympathetic nerve activity and blood pressure in rats. J Physiol. 2009b; 587:5613–5631. [PubMed: 19822543]

Abbott SB, Stornetta RL, Socolovsky CS, West GH, Guyenet PG. Photostimulation of channelrhodopsin-2 expressing ventrolateral medullary neurons increases sympathetic nerve activity and blood pressure in rats. J Physiol. 2009a; 587:5613–5631. [PubMed: 19822543]

Armstrong DM, Ross CA, Pickel VM, Joh TH, Reis DJ. Distribution of dopamine-, noradrenaline-, and adrenaline- containing cell bodies in the rat medulla oblongata: demonstrated by the immunocytochemical localization of catecholamine biosynthetic enzymes. J Comp Neurol. 1982; 212:173–187. [PubMed: 6142061]

Atasoy D, Aponte Y, Su HH, Sternson SM. A FLEX switch targets Channelrhodopsin-2 to multiple cell types for imaging and long-range circuit mapping. J Neurosci. 2008; 28:7025–7030. [PubMed: 18614669]

Berube-Carriere N, Guay G, Fortin GM, Kullander K, Olson L, Wallen-Mackenzie A, Trudeau LE, Descarries L. Ultrastructural characterization of the mesostriatal dopamine innervation in mice, including two mouse lines of conditional VGLUT2 knockout in dopamine neurons. Eur J Neurosci. 2012; 35:527–538. [PubMed: 22330100]

Berube-Carriere N, Riad M, Dal BG, Levesque D, Trudeau LE, Descarries L. The dual dopamine-glutamate phenotype of growing mesencephalic neurons regresses in mature rat brain. J Comp Neurol. 2009; 517:873–891. [PubMed: 19844994]

Bochorishvili G, Stornetta RL, Coates MB, Guyenet PG. Pre-Botzinger complex receives glutamatergic innervation from galaninergic and other retrotrapezoid nucleus neurons. J Comp Neurol. 2011; 520:1047–1061. [PubMed: 21935944]

Broussard JI. Co-transmission of dopamine and glutamate. J Gen Physiol. 2012; 139:93–96. [PubMed: 22200950]

Browning KN, Renehan WE, Travagli RA. Electrophysiological and morphological heterogeneity of rat dorsal vagal neurones which project to specific areas of the gastrointestinal tract. J Physiol. 1999; 517(Pt 2):521–532. [PubMed: 10332099]

Card JP, Sved JC, Craig B, Raizada M, Vazquez J, Sved AF. Efferent projections of rat rostroventrolateral medulla C1 catecholamine neurons: Implications for the central control of cardiovascular regulation. J Comp Neurol. 2006; 499:840–859. [PubMed: 17048222]

Chalmers J, Kapoor V, Mills E, Minson J, Morris M, Pilowsky P, West M. Do pressor neurons in the ventrolateral medulla release amines and neuropeptides? Can J Physiol Pharmacol. 1987; 65:1598–1604. [PubMed: 3690392]

Chen D, Jancovski N, Bassi JK, Nguyen-Huu TP, Choong YT, Palma-Rigo K, Davern PJ, Gurley SB, Thomas WG, Head GA, Allen AM. Angiotensin type 1A receptors in C1 neurons of the rostral ventrolateral medulla modulate the pressor response to aversive stress 21. J Neurosci. 2012; 32:2051–2061. [PubMed: 22323719]

Comer AM, Qi J, Christie DL, Gibbons HM, Lipski J. Noradrenaline transporter expression in the pons and medulla oblongata of the rat: localisation to noradreneric and some C1 adrenergic neurones. Mol Brain Res. 1998; 62:65–76. [PubMed: 9795140]

Depuy SD, Kanbar R, Coates MB, Stornetta RL, Guyenet PG. Control of breathing by raphe obscurus serotonergic neurons in mice. J Neurosci. 2011; 31:1981–1990. [PubMed: 21307236]

Engler KL, Rudd ML, Ryan JJ, Stewart JK, Fischer-Stenger K. Autocrine actions of macrophage-derived catecholamines on interleukin-1 beta 5. J Neuroimmunol. 2005; 160:87–91. [PubMed: 15710461]

Farnham MM, Li Q, Goodchild AK, Pilowsky PM. PACAP is expressed in sympathoexcitatory bulbospinal C1 neurons of the brain stem and increases sympathetic nerve activity in vivo. Am J Physiol Regul Integr Comp Physiol. 2008; 294:R1304–R1311. [PubMed: 18272663]

Gras C, Herzog E, Bellenchi GC, Bernard V, Ravassard P, Pohl M, Gasnier B, Giros B, El Mestikawy S. A third vesicular glutamate transporter expressed by cholinergic and serotoninergic neurons. J Neurosci. 2002; 22:5442–5451. [PubMed: 12097496]

Guyenet PG. The sympathetic control of blood pressure. Nat Rev Neurosci. 2006; 7:335–346. [PubMed: 16760914]

Halliday GM, Li YW, Joh TH, Cotton RG, Howe PR, Geffen LB, Blessing WW. Distribution of substance P-like immunoreactive neurons in the human medulla oblongata: co-localization with monoamine- synthesizing neurons. Synapse. 1988; 2:353–370. [PubMed: 2460960]

Hokfelt T, Fuxe K, Goldstein M, Johansson O. Immunohistochemical evidence for the existence of adrenaline neurons in the rat brain. Brain Res. 1974; 66:235–251.

Li AJ, Wang Q, Dinh TT, Ritter S. Simultaneous silencing of Npy and Dbh expression in hindbrain A1/C1 catecholamine cells suppresses glucoprivic feeding. J Neurosci. 2009; 29:280–287. [PubMed: 19129404]

Li YW, Bayliss DA, Guyenet PG. C1 neurons of neonatal rats: Intrinsic beating properties and α_2-adrenergic receptors. Am J Physiol-Reg Integr Comp Physiol. 1995; 269:R1356–R1369.

Li YW, Guyenet PG, Bayliss DA. Voltage-dependent calcium currents in bulbospinal neurons of neonatal rat rostral ventrolateral medulla: Modulation by α_2- adrenergic receptors. J Neurophys. 1998; 79:583–594.

Lorang D, Amara SG, Simerly RB. Cell-type-specific expression of catecholamine transporters in the rat brain. J Neurosci. 1994; 14:4903–4914. [PubMed: 8046459]

Marina N, Abdala AP, Korsak A, Simms AE, Allen AM, Paton JF, Gourine AV. Control of sympathetic vasomotor tone by catecholaminergic C1 neurones of the rostral ventrolateral medulla oblongata. Cardiovasc Res. 2011; 91:703–710. [PubMed: 21543384]

Martinez-Pena y Valenzuela I, Rogers RC, Hermann GE, Travagli RA. Norepinephrine effects on identified neurons of the rat dorsal motor nucleus of the vagus. Am J Physiol Gastrointest Liver Physiol. 2004; 286:G333–G339. [PubMed: 12936913]

Milner TA, Abate C, Reis DJ, Pickel VM. Ultrastructural localization of phenylethanolamine N-methyltransferase-like immunoreactivity in the rat locus coeruleus. Brain Res. 1989; 478:1–15. [PubMed: 2924106]

Milner TA, Morrison SF, Abate C, Reis DJ. Phenylethanolamine N-methyltransferase-containing terminals synapse directly on sympathetic preganglionic neurons in the rat. Brain Res. 1988; 448:205–222. [PubMed: 3378146]

Morrison SF, Ernsberger P, Milner TA, Callaway J, Gong A, Reis DJ. A glutamate mechanism in the intermediolateral nucleus mediates sympathoexcitatory responses to stimulation of the rostral ventrolateral medulla. Prog Brain Res. 1989; 81:159–169. [PubMed: 2575775]

Moss J, Ungless MA, Bolam JP. Dopaminergic axons in different divisions of the adult rat striatal complex do not express vesicular glutamate transporters. Eur J Neurosci. 2011; 33:1205–1211. [PubMed: 21375596]

Olofsson PS, Rosas-Ballina M, Levine YA, Tracey KJ. Rethinking inflammation: neural circuits in the regulation of immunity. Immunol Rev. 2012; 248:188–204. [PubMed: 22725962]

Petreanu L, Mao T, Sternson SM, Svoboda K. The subcellular organization of neocortical excitatory connections. Nature. 2009; 457:1142–1145. [PubMed: 19151697]

Phillips JK, Goodchild AK, Dubey R, Sesiashvili E, Takeda M, Chalmers J, Pilowsky PM, Lipski J. Differential expression of catecholamine biosynthetic enzymes in the rat ventrolateral medulla. J Comp Neurol. 2001; 432:20–34. [PubMed: 11241375]

Pirnik Z, Mravec B, Kubovcakova L, Mikkelsen JD, Kiss A. Hypertonic saline and immobilization induce Fos expression in mouse brain catecholaminergic cell groups: colocalization with tyrosine hydroxylase and neuropeptide Y. Ann N Y Acad Sci. 2004; 1018:398–404. [PubMed: 15240395]

Ritter S, Bugarith K, Dinh TT. Immunotoxic destruction of distinct catecholamine subgroups produces selective impairment of glucoregulatory responses and neuronal activation. J Comp Neurol. 2001; 432:197–216. [PubMed: 11241386]

Ritter S, Llewellyn-Smith I, Dinh TT. Subgroups of hindbrain catecholamine neurons are selectively activated by 2-deoxy-D-glucose induced metabolic challenge. Brain Res. 1998; 805:41–54. [PubMed: 9733914]

Rogers RC, Hermann GE, Travagli RA. Brainstem pathways responsible for oesophageal control of gastric motility and tone in the rat. J Physiol. 1999; 514:369–383. [PubMed: 9852320]

Rosin DL, Chang DA, Guyenet PG. Afferent and efferent connections of the rat retrotrapezoid nucleus. J Comp Neurol. 2006; 499:64–89. [PubMed: 16958085]

Ross CA, Ruggiero DA, Joh TH, Park DH, Reis DJ. Adrenaline synthesizing neurons in the rostral ventrolateral medulla: a possible role in tonic vasomotor control. Brain Res. 1983; 273:356–361. [PubMed: 6616243]

Ross CA, Ruggiero DA, Joh TH, Park DH, Reis DJ. Rostral ventrolateral medulla: selective projections to the thoracic autonomic cell column from the region containing C1 adrenaline neurons. J Comp Neurol. 1984; 228:168–185. [PubMed: 6480910]

Sawchenko PE, Li HY, Ericsson A. Circuits and mechanisms governing hypothalamic responses to stress: a tale of two paradigms. Prog Brain Res. 2000; 122:61–78. [PubMed: 10737051]

Scott MM, Wylie CJ, Lerch JK, Murphy R, Lobur K, Herlitze S, Jiang W, Conlon RA, Strowbridge BW, Deneris ES. A genetic approach to access serotonin neurons for in vivo and in vitro studies. Proc Natl Acad Sci USA. 2005; 102:16472–16477. [PubMed: 16251278]

Sevigny CP, Bassi J, Teschemacher AG, Kim KS, Williams DA, Anderson CR, Allen AM. C1 neurons in the rat rostral ventrolateral medulla differentially express vesicular monoamine transporter 2 in soma and axonal compartments. Eur J Neurosci. 2008; 28:1536–1544. [PubMed: 18973576]

Sheng M, Kim E. The postsynaptic organization of synapses. Cold Spring Harb Perspect Biol. 2011; 3

Shu Y, Yu Y, Yang J, Mccormick DA. Selective control of cortical axonal spikes by a slowly inactivating K+ current. Proc Natl Acad Sci U S A. 2007; 104:11453–11458. [PubMed: 17581873]

Sorriento D, Santulli G, Del GC, Anastasio A, Trimarco B, Iaccarino G. Endothelial cells are able to synthesize and release catecholamines both in vitro and in vivo. Hypertension. 2012; 60:129–136. [PubMed: 22665130]

Standish A, Enquist LW, Escardo JA, Schwaber JS. Central neuronal circuit innervating the rat heart defined by transneuronal transport of pseudorabies virus. J Neurosci. 1995; 15:1998–2012. [PubMed: 7891147]

Stjarne L, Brundin J. Beta2-adrenoceptors facilitating noradrenaline secretion from human vasoconstrictor nerves. Acta Physiol Scand. 1976; 97:88–93. [PubMed: 5851]

Stornetta RL, Akey PJ, Guyenet PG. Location and electrophysiological characterization of rostral medullary adrenergic neurons that contain neuropeptide Y mRNA in rat. J Comp Neurol. 1999; 415:482–500. [PubMed: 10570457]

Stornetta RL, Guyenet PG. Distribution of glutamic acid decarboxylase mRNA-containing neurons in rat medulla projecting to thoracic spinal cord in relation to monoaminergic brainstem neurons. J Comp Neurol. 1999; 407:367–380. [PubMed: 10320217]

Stornetta RL, Macon CJ, Nguyen TM, Coates MB, Guyenet PG. Cholinergic neurons in the mouse rostral ventrolateral medulla target sensory afferent areas. Brain Struct Funct. 2012

Stornetta RL, McQuiston TJ, Guyenet PG. GABAergic and glycinergic presympathetic neurons of rat medulla oblongata identified by retrograde transport of pseudorabies virus and in situ hybridization. J Comp Neurol. 2004; 479:257–270. [PubMed: 15457502]

Stornetta RL, Sevigny CP, Guyenet PG. Vesicular glutamate transporter DNPI/VGLUT2 mRNA is present in C1 and several other groups of brainstem catecholaminergic neurons. J Comp Neurol. 2002; 444:191–206. [PubMed: 11840474]

Stuber GD, Hnasko TS, Britt JP, Edwards RH, Bonci A. Dopaminergic terminals in the nucleus accumbens but not the dorsal striatum corelease glutamate. J Neurosci. 2010; 30:8229–8233. [PubMed: 20554874]

Sulzer D, Joyce MP, Lin L, Geldwert D, Haber SN, Hattori T, Rayport S. Dopamine neurons make glutamatergic synapses in vitro. J Neurosci. 1998; 18:4588–4602. [PubMed: 9614234]

Sved AF. PNMT-containing catecholaminergic neurons are not necessarily adrenergic. Brain Res. 1989; 481:113–118. [PubMed: 2706454]

Tecuapetla F, Patel JC, Xenias H, English D, Tadros I, Shah F, Berlin J, Deisseroth K, Rice ME, Tepper JM, Koos T. Glutamatergic signaling by mesolimbic dopamine neurons in the nucleus accumbens. J Neurosci. 2010; 30:7105–7110. [PubMed: 20484653]

Tong Q, Ye C, McCrimmon RJ, Dhillon H, Choi B, Kramer MD, Yu J, Yang Z, Christiansen LM, Lee CE, Choi CS, Zigman JM, Shulman GI, Sherwin RS, Elmquist JK, Lowell BB. Synaptic glutamate release by ventromedial hypothalamic neurons is part of the neurocircuitry that prevents hypoglycemia. Cell Metab. 2007; 5:383–393. [PubMed: 17488640]

Trendelenburg AU, Philipp M, Meyer A, Klebroff W, Hein L, Starke K. All three α_2-adrenoceptor types serve as autoreceptors in postganglionic sympathetic neurons. Naunyn Schmiedebergs Arch Pharmacol. 2003; 368:504–512. [PubMed: 14610637]

Witten IB, Steinberg EE, Lee SY, Davidson TJ, Zalocusky KA, Brodsky M, Yizhar O, Cho SL, Gong S, Ramakrishnan C, Stuber GD, Tye KM, Janak PH, Deisseroth K. Recombinase-driver rat lines:

tools, techniques, and optogenetic application to dopamine-mediated reinforcement. Neuron. 2011; 72:721–733. [PubMed: 22153370]

Yamaguchi T, Wang HL, Li X, Ng TH, Morales M. Mesocorticolimbic glutamatergic pathway. J Neurosci. 2011; 31:8476–8490. [PubMed: 21653852]

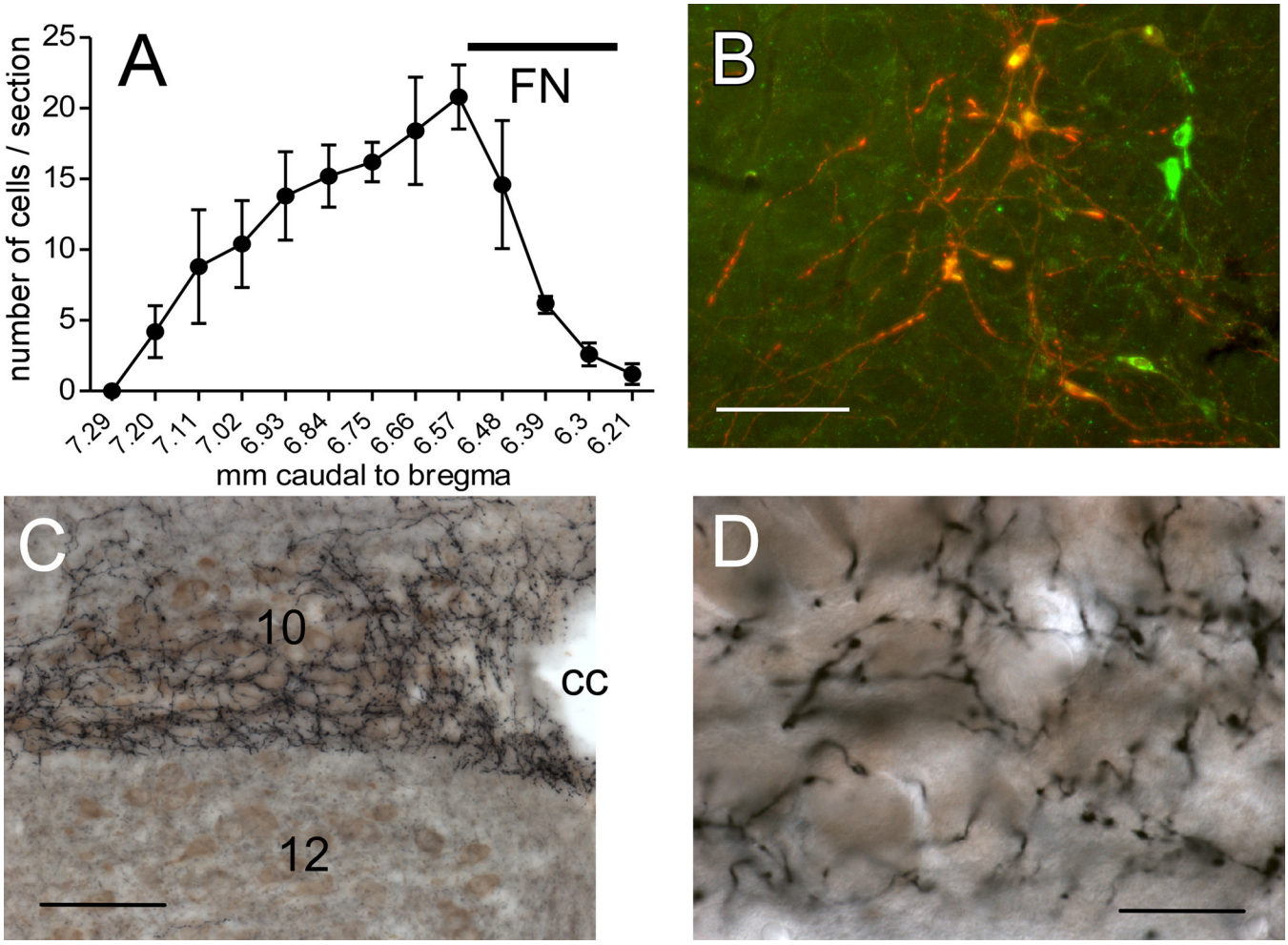

Figure 1. RVLM-Catecholaminergic (RVLM-CA) neurons innervate the dorsal motor nucleus of the vagus (DMV) in DβH-Cre mice

A, Rostrocaudal distribution of mCherry+TH-ir neurons (average of 5 cases). The ChR2-expressing neurons were confined to the RVLM. FN, caudal extent of the facial motor nucleus provided as reference. Dual-labeled neurons appear orange-yellow. Untransfected TH-ir neurons appear green. ***B,*** Photomicrograph of the RVLM one month after injection of AAV2-DIO-ChR2-mCherry into the same region in a DβH-Cre mice. mCherry immunoreactivity (red) is detectable exclusively in tyrosine hydroxylase (TH)-immunoreactive(ir) neurons (green). Scale, 100 μm. ***C,*** Photomicrograph showing the dense plexus of nerve terminals arising from mCherry-ir RVLM-CA neurons. ChR2-mCherry is visualized with the nickel-DAB method resulting in a black color. Choline acetyl-transferase (ChAT)-immunoreactivity is visualized with DAB resulting in a brown color. Note the dense terminal field in the DMV (10) that avoids the hypoglossal nucleus (12). cc, central canal. Scale, 200 μm. ***D,*** Higher power photomicrograph of the DMV innervation seen in *C* showing fibers and synaptic boutons arising from ChR2-expressing RVLM-CA neurons in close proximity of the DMV cholinergic neurons. Scale, 30 μm.

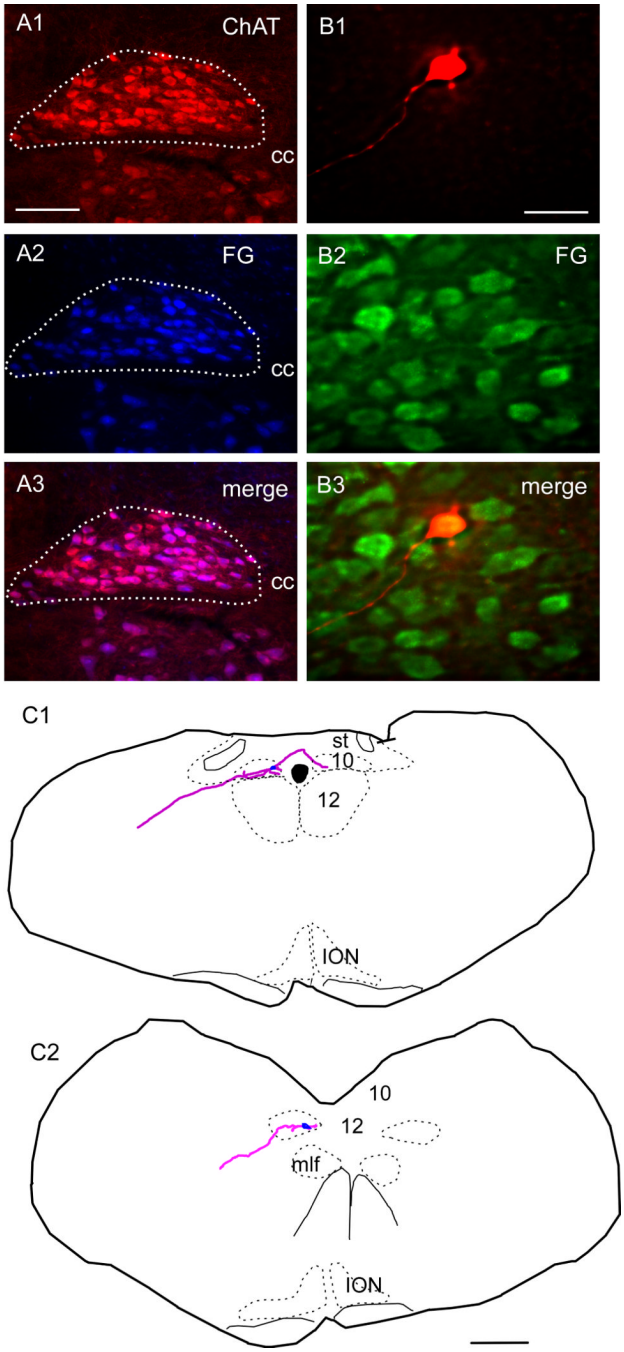

Figure 2. Verification that Fluoro-Gold (FG) labels ChAT neurons in the DMV and that the recorded neurons are vagal premotor neurons

A1–A3, Photomicrograph of DMV illustrating that ChAT-ir neurons (red) in DMV(A1) are also FG positive (blue) (***A2***). ***A3,*** Merged image of ***A1*** and ***A2***, double labeled neurons appear pink. Scale in ***A1***, 100 μm, applies to ***A1–A3***. ***B,*** Example of a slice reacted for immunohistochemistry to reveal the biocytin label (***B1***) showing the cell is also FG-ir (green, ***B2***). ***B3,*** Merge of ***B1*** and ***B2*** showing the cell is within the DMV and also FG, thus projecting outside the brain. Scale in ***B1***, 50 μm, applies to ***B1–B3***. ***C1, C2,*** Illustrations of biocytin filled neurons recorded in slices and reconstructed showing the dendrites and axon projecting towards the periphery of the section. Scale in ***C2***, 0.5 mm applies to ***C1–C2***.

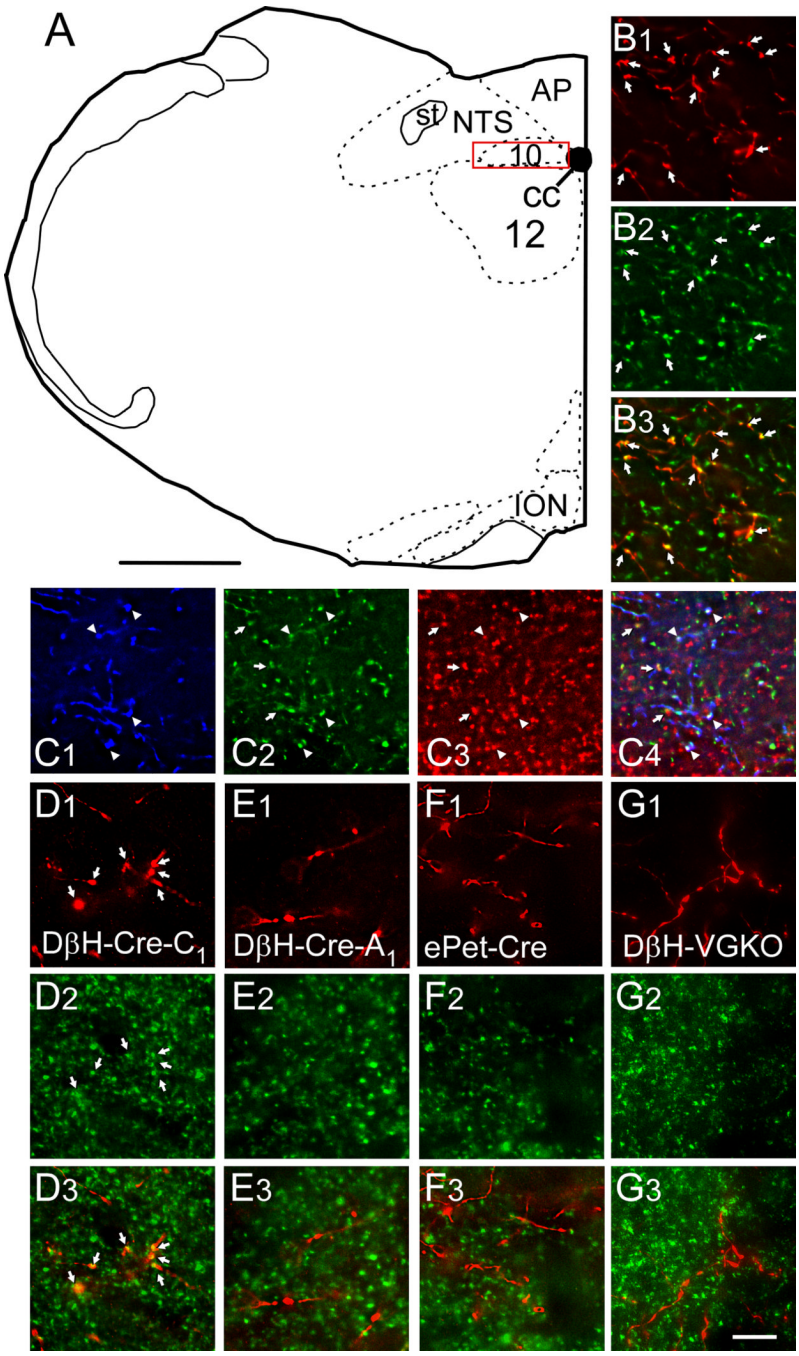

Figure 3. VGLUT2 is present in DMV varicosities that originate from RVLM-CA neurons but is absent from those that emanate from A1 noradrenergic and raphe serotonergic neurons

A, Drawing of mouse brain coronal hemisection at ~7.64 mm caudal to bregma. The red box represents the region of the DMV where axonal varicosities were counted and the photomicrographs were taken. Scale in ***A***, 500 μm. ***B1,*** Photomicrograph of mCherry-ir terminals (red) in the DMV from a DβH-Cre mouse injected in RVLM with DIO-ChR2-mCherry AAV2. ***B2***, TH-ir varicosities within the same field. ***B3,*** Merged image (***B1*** + ***B2***) showing that all the mCherry-ir varicosities are yellow, i.e. contain TH. ***C***, Same experiment as in ***B*** but revealing mCherry with a rabbit secondary tagged with Dylight 649 and pseudocolored blue (***C1***) and both TH-ir (green, ***C2***) and VGLUT2-ir varicosities (red, ***C3***).

C4, Merged image (***C1*** + ***C2*** + ***C3***) showing triple labeled terminals (appearing white, arrowheads) as well as terminals double labeled only for TH and VGLUT2 (appearing yellow, arrows). ***D1,*** Photomicrograph of mCherry-ir terminals (red) in the DMV from a DβH-Cre mouse injected in RVLM with DIO-ChR2-mCherry AAV2. ***D2***, VGLUT2-ir varicosities within the same field. ***D3,*** Merged image (***B1*** + ***B2***) showing that all the mCherry-ir varicosities are yellow, i.e. contain VGLUT2. ***E,*** Similar experiment to ***B*** except the DβH-Cre mouse was injected in the A1 region (caudal VLM). ***E1,*** mCherry ***E2,*** VGLUT2 ***E3,*** Merge of ***C1*** + ***C2***. Note that the mCherry-ir varicosities are red, i.e. are not VGLUT2-ir. ***F,*** Similar experiment to ***B*** except the AAV2 was injected into the raphe obscurus of an ePet-Cre mouse. ***F1,*** mCherry ***F2,*** VGLUT2 ***F3,*** Merge of ***F1*** + ***F2***. Note that the mCherry-ir varicosities are red, i.e. are not VGLUT2-ir. ***G***, Similar experiment to ***B*** except the AAV2 was injected into the RVLM of a DβH-Cre$^{(Cre/0)}$; Vglut2$^{(flox/flox)}$ mouse (DβH -VGKO). ***G1,*** mCherry ***G2,*** VGLUT2 ***G3,*** Merge of ***G1*** + ***G2***. Note that the mCherry-ir varicosities are red, i.e. are not VGLUT2-ir. Abbreviations: 10, dorsal motor nucleus of the vagus; 12, hypoglossal motor nucleus; AP, area postrema; cc, central canal; DβH, dopamine beta hydroxylase; ION, inferior olivary nucleus; NTS, nucleus of the solitary tract; st, solitary tract. Scale in ***G3*** applies to ***B–G***, 10 μm.

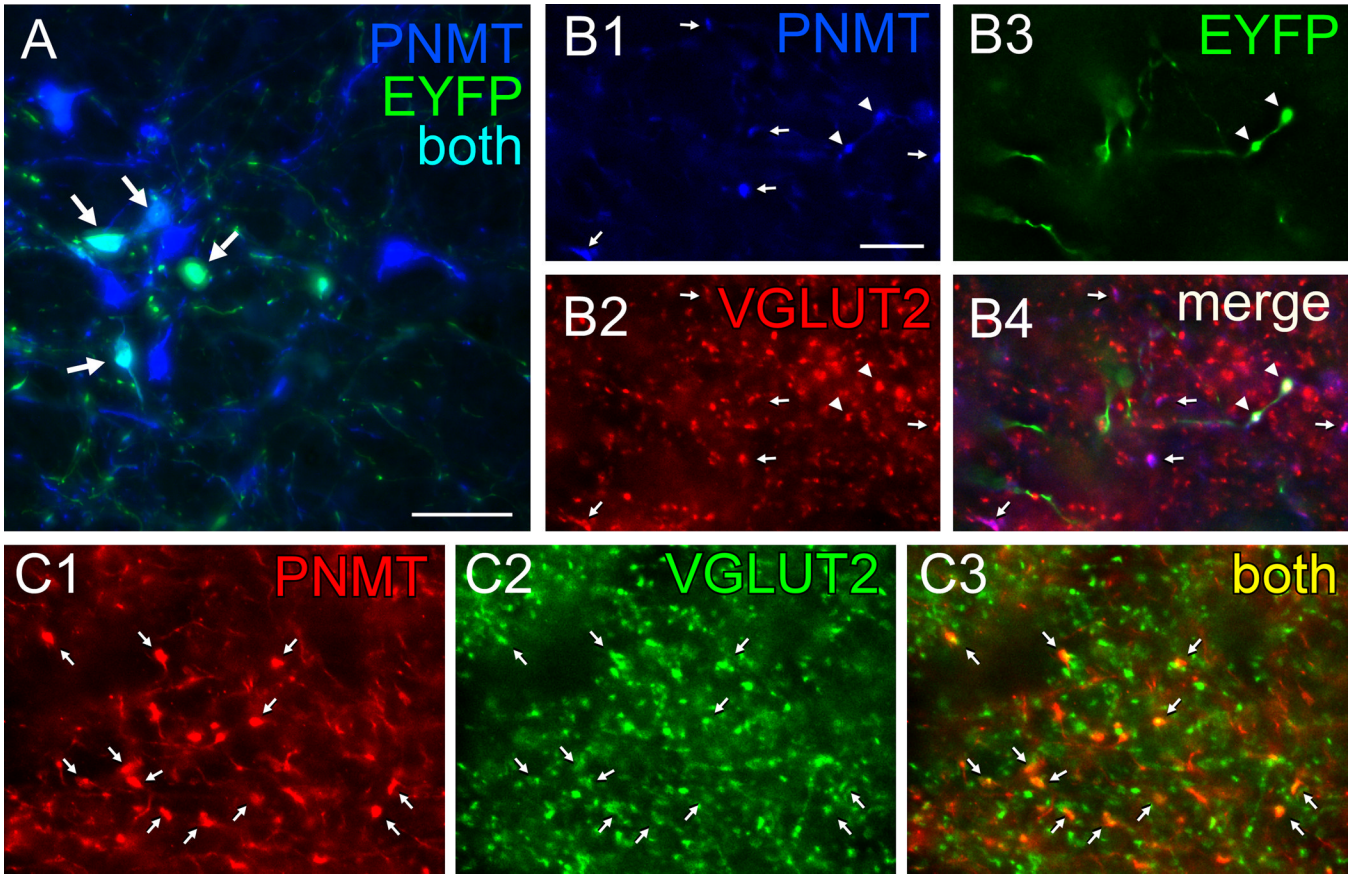

Figure 4. Axonal varicosities from C1 neurons in rat DMV contain PNMT and VGLUT2

A, Photomicrograph showing that injection of AAV2-DIO-EYFP into the RVLM drives expression of EYFP in C1 (PNMT-ir) neurons in TH-Cre rats. EYFP immunoreactivity is in green and phenylethanolamine-N-methyl transferase (PNMT)-ir is in blue. Double labeled neurons appear aqua (arrows). Scale, 50 μm. ***B***,Virtually all adrenergic varicosities (PNMT-ir, blue) within the DMV (***B1***, denoted by arrows or arrowheads) are also glutamatergic (VGLUT2-ir, red) (***B2***). The EYFP terminals (green) (***B3***, arrowheads) originating from C1 RVLM neurons are both adrenergic (red) and glutamatergic (green). ***B4,*** Merge of ***B1–B3***. Triple labeled terminals (arrowheads) appear white. Double-label terminals (PNMT + VGLUT2) appear purple (arrows) when the colors are merged. ***C,*** Adrenergic terminals in DMV are also glutamatergic in naïve TH-Cre rats (no AAV2 injection). Adrenergic nerve terminals (PNMT-ir, red) located in DMV (***C1***) are also glutamatergic (VGLUT2-ir, green) (***C2***), arrows. These terminals appear yellow when the colors are merged in ***C3*** (arrows). Note that practically all the PNMT-ir terminals are also VGLUT2-ir similar to the virus-injected rat shown in ***B***. Scale in ***B1***, 10 μm applies to ***B–C***.

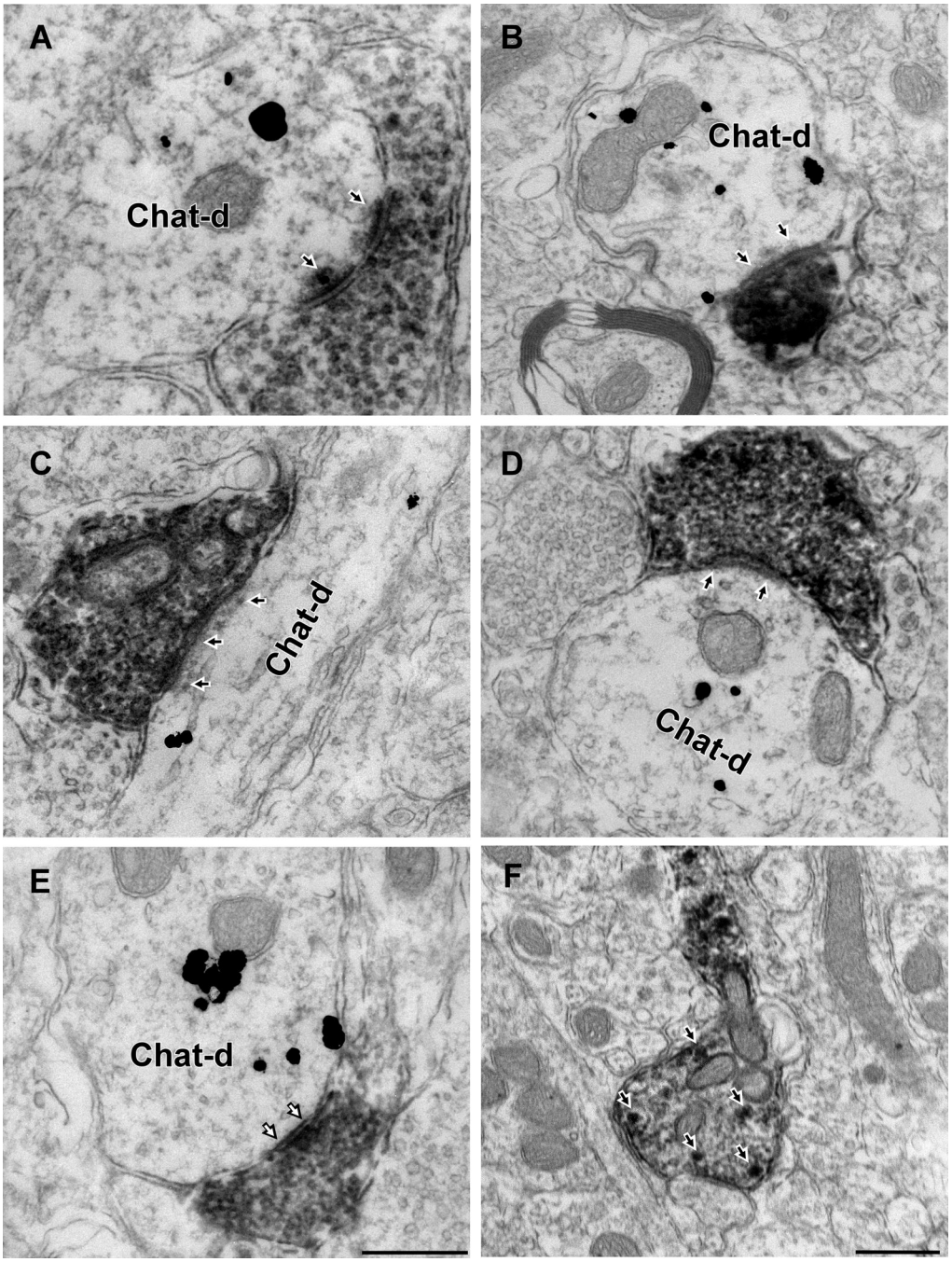

Figure 5. RVLM-CA neurons make synapses with DMV cholinergic neurons

A–D, Electron micrographs of the DMV from DβH-Cre mice injected with DIO-ChR2-mCherry AAV2 in RVLM. mCherry-ir axonal varicosities labeled with immunoperoxidase reaction product make synapses onto dendrites containing gold-silver labeling for ChAT. The postsynaptic density (black arrows), indicate that these synapses are asymmetric and presumably glutamatergic. ***E,*** Example of symmetric synapse (white arrows) between mCherry-ir (peroxidase) terminal and ChAT-ir (gold) dendrite. ***F,*** Example of mCherry-positive axon containing dense core vesicles (white arrows) reminiscent of catecholaminergic terminals. Scale in ***E***, 0.5 μm applies to ***A–E***. Scale in ***F***, 0.5 μm.

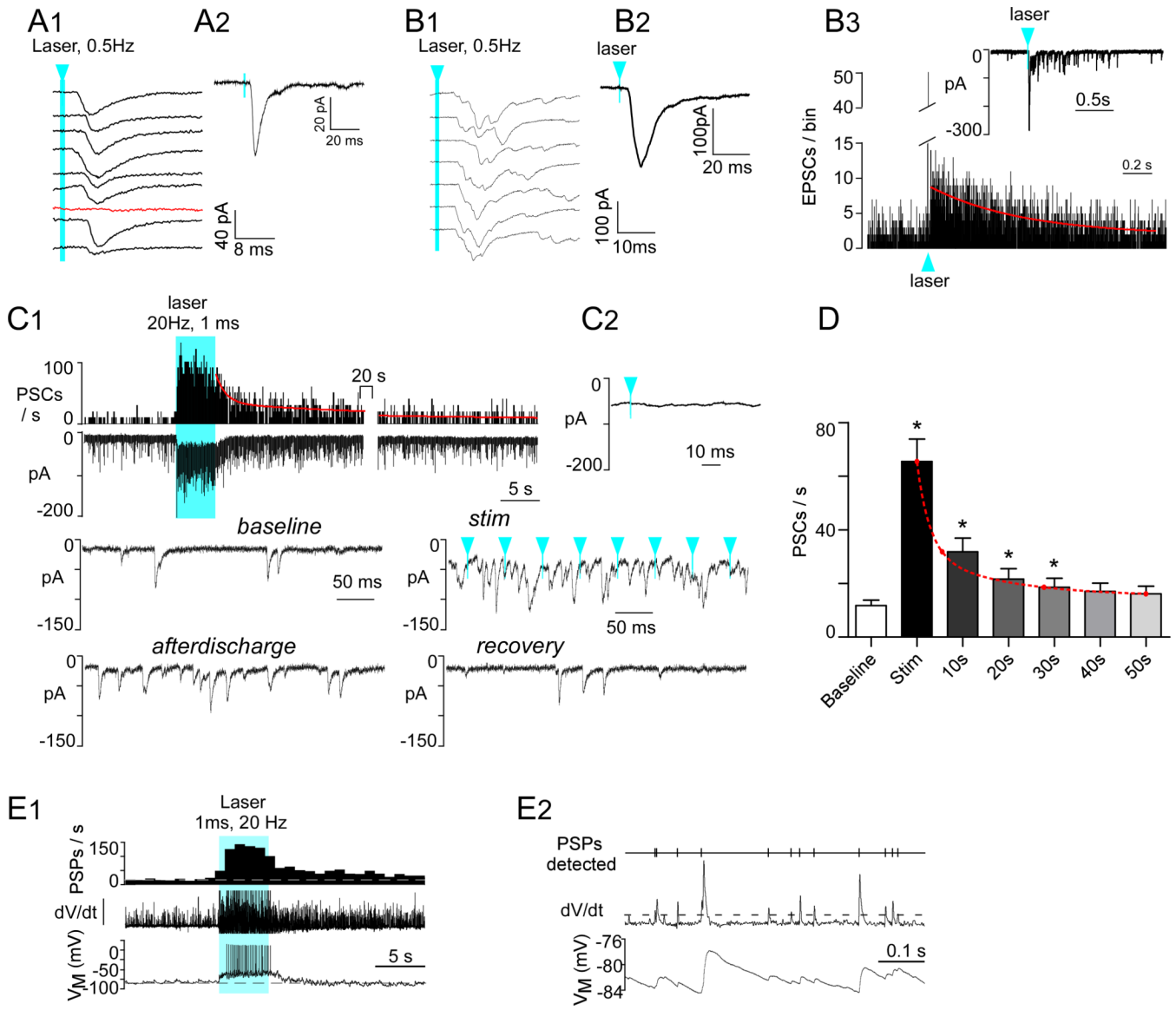

Figure 6. Photostimulation of ChR2-labeled axons produces PSCs in DMV neurons and increases their discharge rate

A1, Compound PSC (note variable latency) evoked in a DMV neuron clamped at −79 mV by nine consecutive 1 ms light flashes (473 nm) delivered at 0.5 Hz. The red trace denotes a failure. Blue arrowhead and line indicates time of laser onset throughout figure. ***A2,*** Event-triggered average of the PSCs evoked in the cell shown in *A1* (75 stimuli). ***B1***, Compound PSC evoked in another DMV neuron (VM −79 mV) by nine consecutive 1 ms light flashes (473 nm) delivered every 2 seconds. This second example illustrates a larger and more multiphasic response. ***B2***, Event-triggered average of the EPSC evoked in the cell shown in *B1* (75 stimuli). ***B3***, The inset shows the EPSC after-discharge that follows the large initial EPSC and the main graph is a peri-event histogram depicting the probability of occurrence of EPSCs following the laser flashes. The red line is a single exponential with a time constant of 0.6s that fits the kinetics of the after-discharge with a probability of 0.9. ***C1***, Top trace: integrated rate histogram of the PSC frequency before during and after photostimulation (20 Hz, 1 ms, train duration 5 s, laser on time represented by solid blue block). Second trace from top, original recording obtained from DMV neuron clamped at

V_M −79 mV. Lower traces, higher resolution excerpts from the original recording. Note that, during high frequency photostimulation, the evoked PSCs are asynchronous with respect to the light pulses. Solid blue block indicates period of photostimulation. ***C2***, Event-triggered average of the PSCs evoked by photostimulation (100 light pulses). Note that the trace is flat indicating asynchrony between PSCs and light pulses. ***D***, Group data showing the average kinetics of the after-discharge (N= 16 neurons). Asterisks indicate $p < 0.001$ between group and baseline except 30 s, $p<0.05$. ***E1***, Response of a DMV neuron to photostimulation of RVLM catecholaminergic neuron input (1ms, 20 Hz, 5s). Bottom trace, original current clamp recording (−10 pA bias current injected to silence the cell). Middle trace, first differential of original trace to highlight PSPs. Top trace, PSP frequency (integrated rate histogram, 1 s bin). Period of photostimulation is indicated by solid blue block. ***E2***, High resolution excerpt illustrating (from the bottom up) the original recording, the first differential used to detect PSPs and analyze their frequency (dotted line, detection threshold) and the detected PSPs.

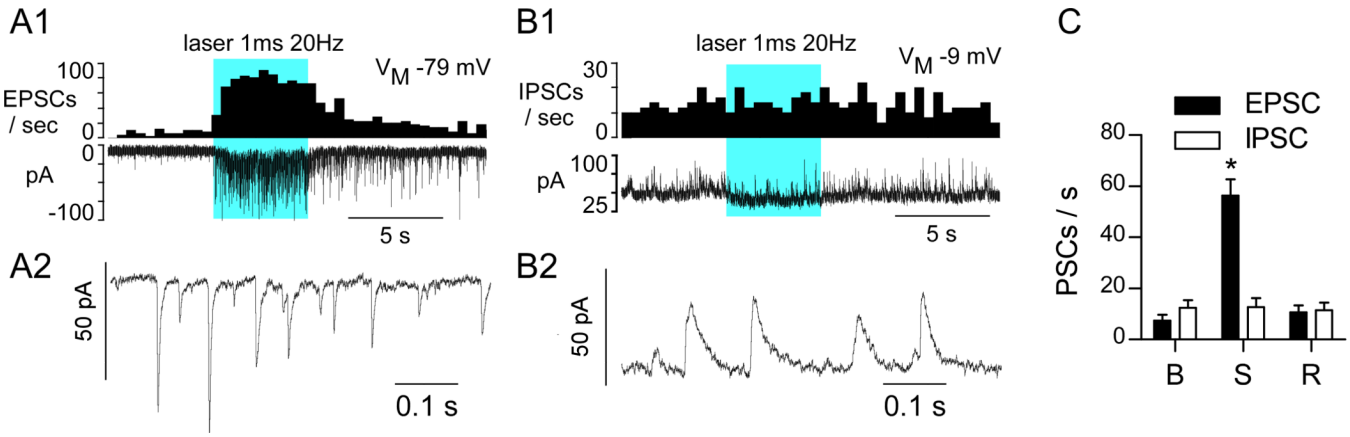

Figure 7. Photostimulation of ChR2-expressing axons produces exclusively EPSCs in DMV neurons

A1, DMV neuron voltage clamped at V_M −79 mV (cesium chloride filled electrode). Top trace EPSC frequency (integrated rate histogram with 0.5 s bin), bottom trace original recording. Solid blue block represents the period of photostimulation. ***A2***, Excerpt of EPSCs recorded during the early part of the after discharge. ***B1***, Same neuron voltage clamped at V_M −9 mV. Top trace illustrates the lack of change of IPSC frequency during photostimulation, bottom trace is the original recording. ***B2***, Excerpt of the recording trace obtained during the stimulation period. ***C***, Group data (N= 9 neurons) showing inhibitory an excitatory PSC frequency at baseline (B), during the 20Hz stimulus (S), and after full recovery (R); asterisks ($P<0.0001$).

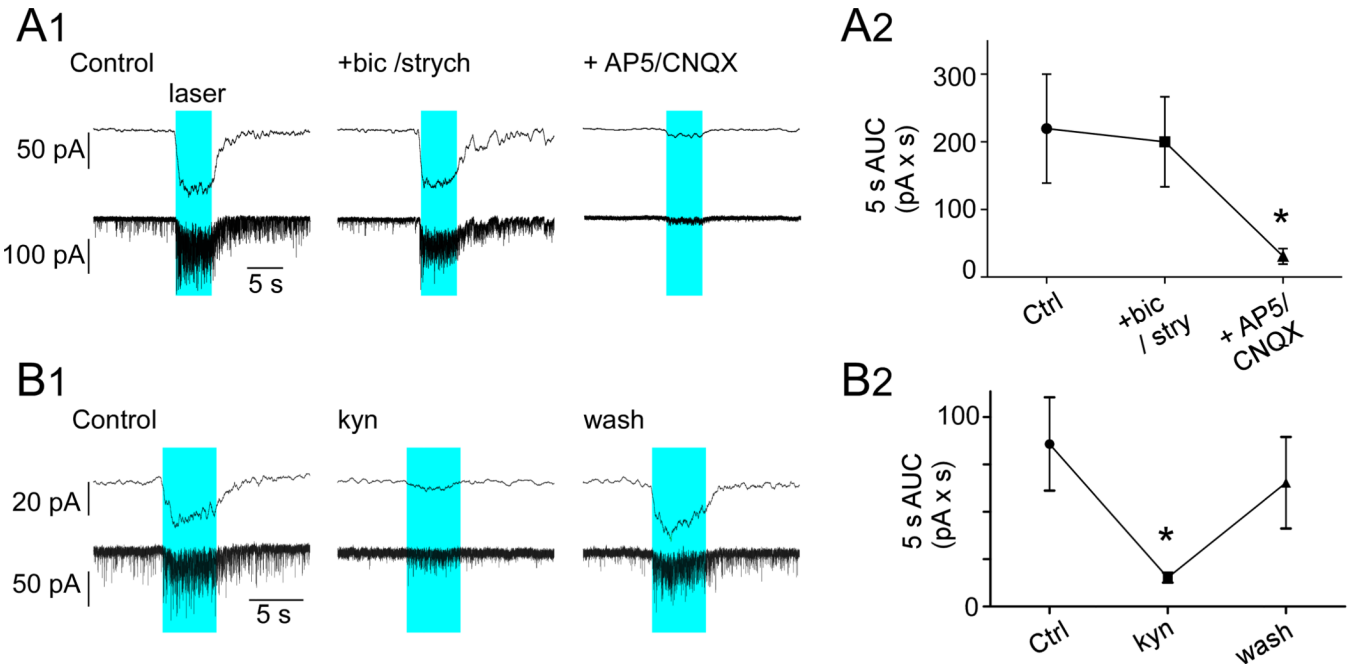

Figure 8. EPSCs evoked in DMV neurons are glutamatergic

A1, Response of a DMV neuron clamped at V_M −79 mV to photostimulation (1ms, 20 Hz, 5 s; blue block represents period of photostimulation). From left to right, control response, response following application of bucuculline (bic, 10μM) and strychnine (strych, 20μM) and response after further addition of ionotropic glutamate receptor blockers AP5 (50 μM) and CNQX (10 μM. Bottom traces, original recordings; top traces low-pass filtered traces (5 Hz). ***A2***, Group data (N = 4). Area under the curve (AUC) obtained from the original recording trace. Asterisk indicates statistical significance from both control and bicuculline/ strychnine ***B1***, Response of a DMV neuron clamped at V_M −79 mV to photostimulation (1ms, 20 Hz, 5 s). From left to right, control response, response following application of kynurenate (kyn, broad-spectrum ionotropic glutamate receptor antagonist, 1mM). Bottom traces, original recordings; top traces low-pass filtered traces (5 Hz). ***B2***, Group data (N = 7). AUC obtained from the original recording traces. Asterisk ($P<0.05$) indicates statistical significance from both control and recovery period.

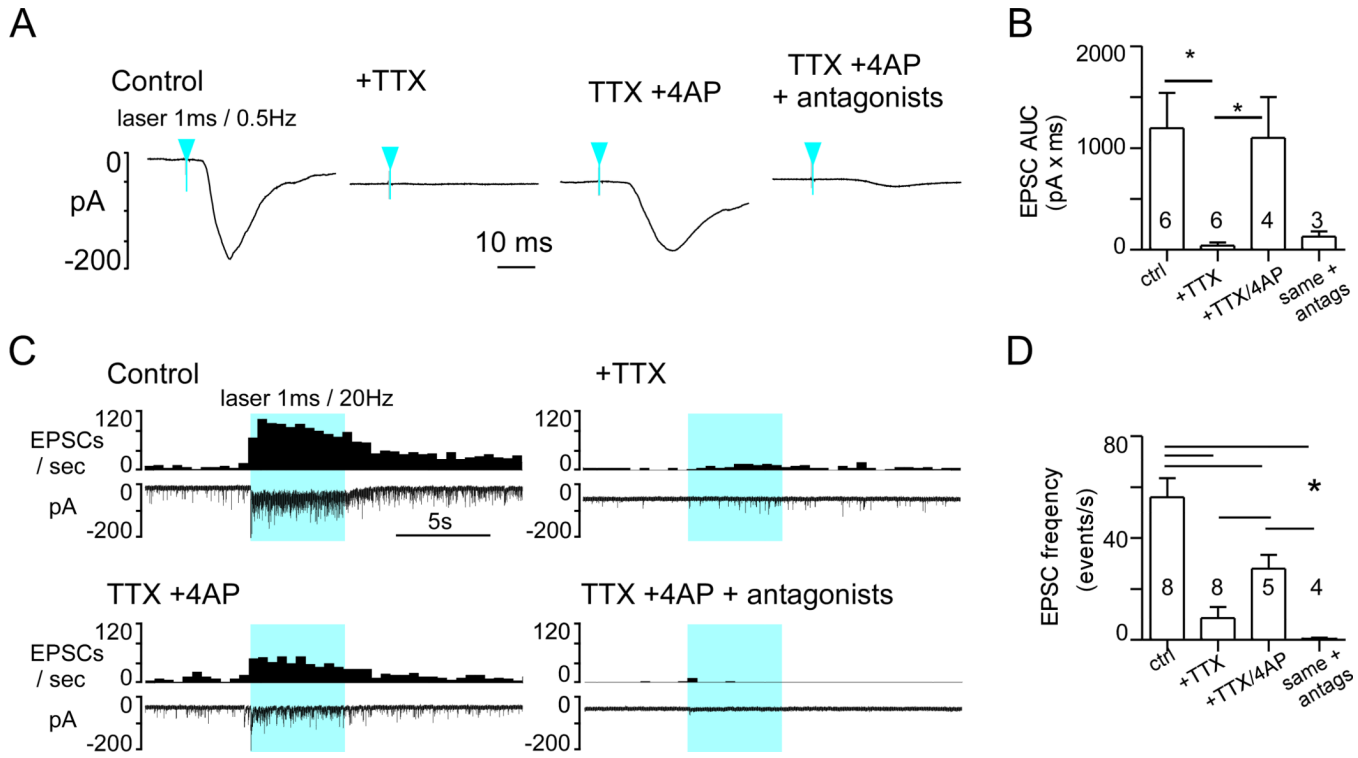

Figure 9. Photostimulation of ChR2-expressing fibers activate DMV neurons after action potential blockade

A, EPSC evoked in a DMV neuron (V_M: −79 mV) by 1 ms light pulses at 0.5 Hz (average of 75 consecutive stimuli) before any drug (left trace), following tetrodotoxin application (TTX, 1μM), after addition of 4-aminopyridine (TTX + 4-AP, 100μM) and in the presence of TTX, 4-AP and glutamatergic antagonists CNQX and AP5. Blue arrowheads indicate time of laser onset. ***B,*** Group data (N= 6 neurons). Asterisks indicate significant differences between groups joined by horizontal bars. ***C***, Experiment illustrating the effect of the same sequence of drug application on the response of a DMV neuron to a train of high frequency photostimulation (1 ms, 20 Hz, 5 s). Solid blue block indicates period of photostimulation. ***D***, Group data (N= 8). Asterisks indicate significant differences between groups joined by horizontal bars.

Table 1

Synaptic contacts formed by mCherry-ir terminals and ChAT-ir neurons in DMV

Mouse	Primary Antibody	DsRed terminals	Synapses (%)	Asymmetric (%)	Symmetric (%)
N=5	DsRed/Rabbit ChAT/Goat	113	65 (59%)	48 (74%)	17(26%)